
Check for updates

measured

(1)

production.
mage will be
teel ~10^{-5} of
this leads to a
e higher D re-

2. Experimental setup

Polished ($R_a \leq 20$ nm) $10 \times 10 \times 5mm^3$ samples with a 1 mm step for clamping are made from Plansee ITER grade 99.98% W with 10 μm times 200 μm elongated grains directed into the sample and steel sheet metal (HiperFer batch FM5 17Cr5). Only thin (<100 nm) damage layers due to polishing were observed by FIB/SEM analysis in similar samples before. No pre-outgassing of residual hydrogen is conducted. The sample irradiation is done in a 1.7 MV tandem DC accelerator in combination with a triple-quadrupole focus magnet and a chamber usually used for ion beam analysis (IBA). The chamber provides a pressure of $8 \pm 2 \times 10^{-8}$ mbar during irradiation. The spot-size can be adjusted via the magnet configuration. The chamber features a 4-axis nano-manipulator with 10 nm resolution, a pA-metre (Keithley 6487) and a tele-centric observation camera with 20 μm resolution. The pA-metre measures the proton dose with a 120 V secondary electron suppression bias on the sample. A software integrates the current, yielding the collected charge. IBA detectors are dismounted prior to irradiation due to the produced neutron radiation quickly damaging the detectors. The deuterium retention is measured in the same setup later.

For spot-size measurement, scintillating $LiAlO_2$ single crystals are placed on the sample holder and the spot-size is derived from the camera image. Average proton currents of about 600 nA are applied for irradiation. For beam spot size measurement, the beam current is reduced to ~30 nA via a reduction of the stripper gas density. Fig. 1 illustrates the typical beam spot of 250 to 550 μm edge length, showing negligible variation of the intensity over the spot area. Variation of the beam current density confirmed the scintillator operated below saturation. The sample temperature is measured via a type-K thermocouple attached to the sample back during irradiation. Due to the excessive heat flux of the focussed ion beam, the irradiation spot reaches a temperature up to 30 K (W) and 104 K (steels), respectively, above the backside one, according to ANSYS 19.1 simulations with fixed backside temperature, 1.5 W beam load on a 0.3 mm spot.

For DPA calculation the SRIM 2013 code in the *Quick Calculation of Damage* mode is used according to agreed standards [9,10]. The calculation is run for 10^5 particles. We use the output number "Total Target Vacancies", which is equivalent to an integral over the graphs of Fig. 2, as the displacements per ion (DPI) in the sense of Eq. (1). The DPI of 2960 keV protons in W is 15.5 with a range of 25.8 μm using a displacement threshold of 50 eV [11]. In a steel of similar composition to Eurofer-97 using thresholds of 28 eV for Cr and 17 eV for Fe a DPI of 43.6 with a range of 34.9 μm is calculated. These displacement energies/thresholds of 17 eV (Fe), 28 eV (Cr), and 50 eV (W) are used throughout this work if not stated otherwise. In order to cut the effect of the Bragg-Peak (see Fig. 2), the DPI calculation is restricted to a depth/range R of 13.8 μm in W (3.5 DPI) and 18 μm in steel (8.6 DPI). The ranges correspond to an increase of the DPI per length of 20% above the surface value, representing the range in this work considered to be homogeneously damaged. For this procedure the first 3 points are excluded due to numerical problems at the surface as SRIM claims itself. tention as shown below. Different irradiation temperatures and damage physics complicate a direct comparison of the damage results at the same DPA values given here with literature sources using other projectile types. Neutrons irradiate homogeneously down to large depth while heavy ions reach down to only 1–2 μm. 3 MeV protons irradiation lies in between. Heavy ions offer high DPA rates while neutrons reach orders of magnitude lower values. The heat load limits the proton induced DPA rate in this study to a value slightly below typical heavy ion experiment values. These fundamental differences between the three irradiation options will lead to a slightly different damage behaviour in the sense of produced defect types, quantities, and their interaction/annihilation (which relates to their volume density and production rate).

The practical problems of light ion irradiation not only lie in the application of relevant doses requiring ion focussing optics, but also in restrictions of the later use in regular, non-active laboratories for post analysis. The problem occurs with steels and W alike, since both Fe and W feature isotopes with (p, n) reactions with thresholds < 2 MeV. For a legal and safe handling of samples, two different energies are compared in terms of activity and damage produced, see Table 1. 3 weeks after irradiation, the samples are analysed via a high purity germanium (HPGe) gamma spectroscopy detector with 2 h counting time. Due to the close reaction thresholds, the effect of energy is significant, with a factor 5 in activity between 2.96 and 3.5 MeV. In contrast to HiperFer, Eu-97 contains vanadium, leading to additional production of Cr-51 not seen in HiperFer. Also the W content (leading to Re-184) of HiperFer exceeds the W content of Eu-97 by a factor 3, leading to higher Re-184 activity. Due to radiation protection aspects, 2.96 MeV is selected for the further studies, allowing to release samples from the accelerator laboratory after 2 weeks cooling. If even lower activity is desired the cooling times increase drastically due to the rather long half-lives of the isotopes listed in Table 1.

For the plasma exposures, the hot-cathode linear arc-plasma device PSI-2 is used [12]. High purity D_2 plasmas are employed by introducing D_2 gas with 99.8% (99.9999% D + H). The PSI-2 base pressure is $8 \pm 3 \times 10^{-8}$ mbar (dominated by H_2O) in all experiments. The impurity content present leads to a few $10^{19}/m^2$ O and C atoms on all samples after exposure, but their impact on the total retention is neglected. The samples are exposed on the axial manipulator with a W masque. Individual sample temperatures are recorded with an InSb infrared camera and a black body reference hole in each sample [13]. All samples temperatures are kept below 420 K. The plasma is seen to have the typical hollow profile of PSI-2 with maximum density and temperature about 25 mm away from the plasma centre and about 1/4 of the peak flux values in the centre and an exponential decay with ~10 mm decay length on the outside. The selected plasma scenario provides a peak flux density of $2.1 \pm 0.5 \times 10^{21}$ D/m^{2}s at an electron temperature of about 8 eV for 4 h resulting in a fluence of $3 \pm 0.8 \times 10^{25}$ D/m^2. A bias of 65 V is applied to the sample holder resulting in ~40 eV ion impact energy. According to the Langmuir probe data, a large spatial variation of flux densities up to a factor 3

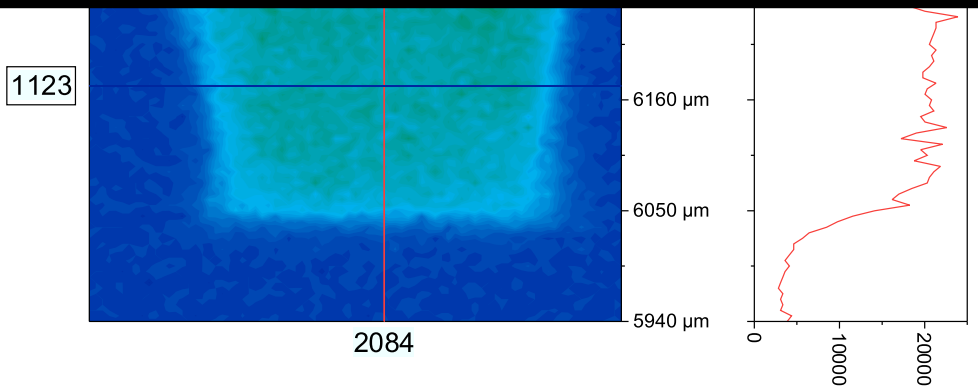

Fig. 1. Exemplary camera image of the irradiation spot scintillation light intensity. Variations of 7% over the spot area and a slight spot deformation are visible.

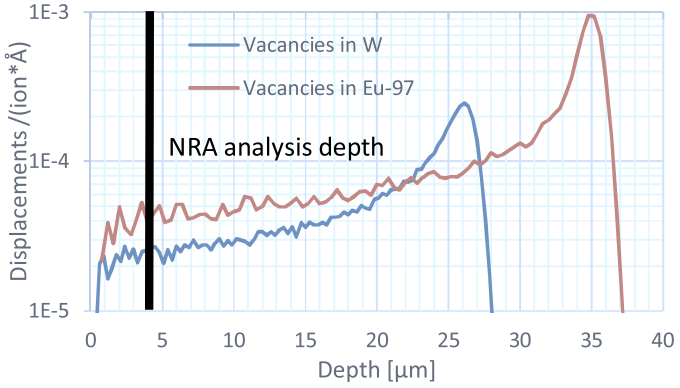

Fig. 2. SRIM calculated displacement damage (Vacancies by ions + recoils) depth profiles induced by 2960 keV protons. Within the range of NRA retention analysis, the damage can be considered constant within the given NRA analysis uncertainties.

below the stated maximum is present on the sample during exposure, due to the hollow flux profile of PSI-2.

After plasma exposure, the retention is analysed via 2.96 MeV ^{3}He ion-beam analysis. The beam is focused to a spot size of 150–200 µm, about half the irradiation spot diameter. The irradiation spots are invisible in the positioning camera, hence camera images acquired during the irradiation are used for reproducing the position based on markings and the grid-like irradiation spot pattern. The accuracy of sample installation and beam localisation limit the positioning to about ± 100 µm accuracy. In this window, the exact position of highest measured D retention is selected, but a systematic uncertainty of the positioning uncertainty in connection with the small spots remains.

A 500 µm thick Si-detector is used for Rutherford-backscattering spectrometry (RBS) and determination of the Particles*Sr value to an accuracy of ± 5%. A known solid angle ratio of 12.8 ± 0.5 transfers this value to the second 1500 µm thick NRA detector at the same reaction angle of 150°. A 12.5 µm thick Kapton foil blocks the RBS part in the NRA detector. The spectra are analysed via SimNRA 7.02 [2]. For data evaluation, cross-sections for ^{12}C(^{3}He, p)^{14}N [3] and D(^{3}He, p)^{4}He [14] are applied. The measurement is done about 4 weeks after exposure with storage in air. Statistical measurement uncertainties due to counting, geometry, and Particle*Sr sum up to 15%. Only in the case of un-irradiated steels low counting statistics increase the uncertainty to 35%. The main source of systematic uncertainty for the NRA based retention analysis lies in systematic problems of the alignment of the invisible proton irradiation spot with the ^{3}He analysis beam. Due to the sub-mm irradiation spot sizes, alignment errors of 0.15 mm (sample

Table 1
Post irradiation activity of all detected nuclides measured by HPGe spectroscopy.

	Activity [Bq/mC]						Irradiation	
Experiment	Cr-51	Mn-54	Co-57	Co-58	Re-184	Sum	Damage rate	Range
Eu-97, 2.96 MeV	10.30	0.85	11.37	0.52	0.56	23.59	0.24 DPA/mC	34.9 µm
Hiperfer, 3.5 MeV	0.0	7.19	32.38	3.68	3.76	47.02	0.2 DPA/mC	45.6 µm

The activation at 2.96 MeV is significantly lower compared to 3.5 MeV. The damage rates were calculated for the homogeneous range (DPA within 20% of the surface value) and a spot of 0.5 mm diameter. All samples feature negligible dose rates <1 nSv/h. Activities have an uncertainty of ± 26%, except for Cr-51 with ± 46%, originating from HPGe counting statistics.

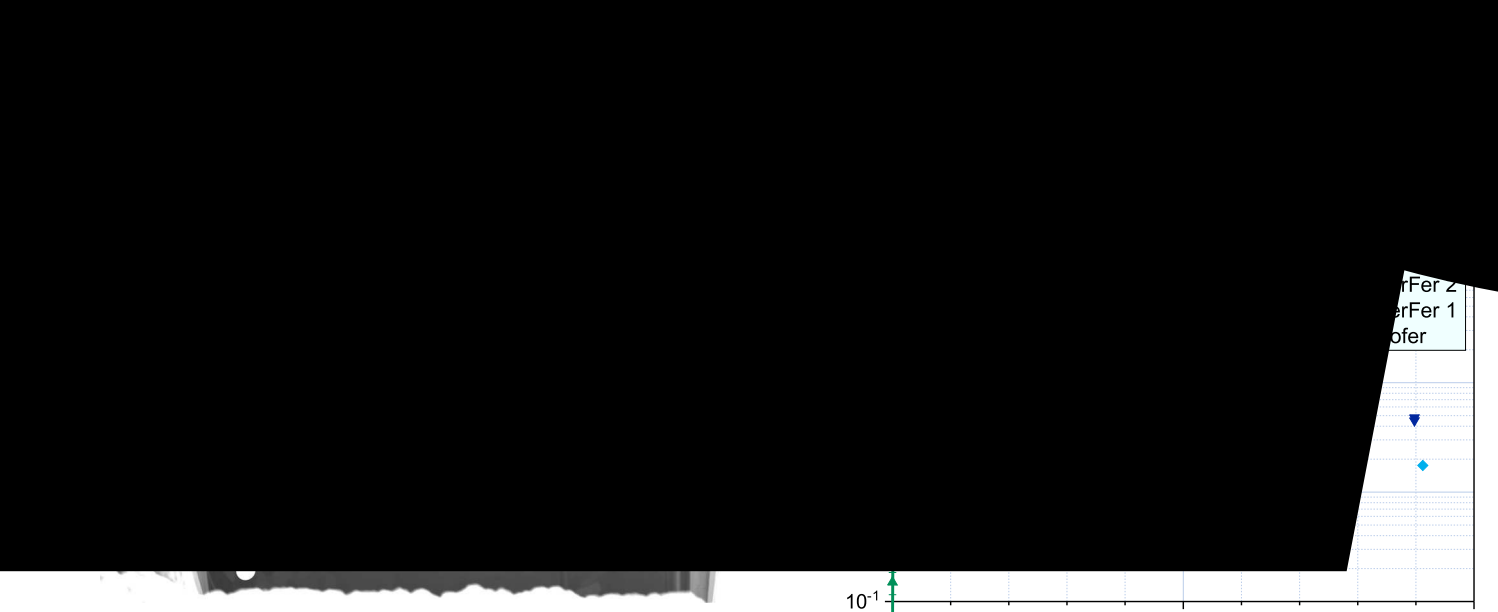

Fig. 3. Exemplary FIB cut in a tungsten sample to 30 µm depth. No sub-surface blisters indicating strong hydrogen retention and mechanical stress can be observed here. Total charge: 1970 µC on 240 × 310 µm beam spot equivalent to ~0.2 DPA dose. Average irradiation current of 573 nA.

Fig. 5. Plot of the relation between surface near retention (~4 µm) and DPA together with exponential fits. Samples of the same material show similar behaviour. The large scatter of the irradiated spots in Eu97 prevents a fitting.

installation tolerance) were seen to change the measured retention by 50%. This absolute systematic uncertainty has to be understood as a constant factor to each set of irradiation spots since all of them were induced and analysed within a single run in one day on a single sample with a given pattern. Within the set, only the relative statistical uncertainties are relevant. In other words: All spots in one sample are equally well/badly aligned.

3. Results

The irradiation potentially introduces modifications to the metal surfaces. For the chosen experimental conditions, no blisters appeared, in contrast to [15]. Fig. 3 shows a representative focussed ion beam (FIB) cut in W down to a depth a few µm deeper than the proton range with no morphological changes observed. With slightly lower irradiation temperatures, irradiation spot sized blisters together with surface elevation were seen in preparatory experiments in W, though. From this we assume, a blister always manifests together with a surface elevation and as all irradiation spots remained flat no blisters are present. Electron microscopy (SEM) in Fig. 4 shows the development of a sparce crack network in W already at the smallest DPA level of 0.0065. The cracks have a width of 50–150 nm and form islands of several uncracked grains of about 50–100 µm in diameter (Fig. 4 right). Besides the cracking in the irradiated W spots, no further changes in surface morphology are visible after irradiation or plasma exposure. With the steels no changes are visible at all.

Ion beam analysis yields the deuterium retention in the irradiated and in un-irradiated reference spots (0 DPA). Fig. 5 and the appendix list the retention and damage values investigated. The depth analysis shows minor surface contaminations of C and O typical for PSI-2 D_2-plasma exposures. D depth profiles measured with a resolution of 2 µm show a decay in retention already in the first 4 µm in W. The first 2 µm contain 1.4 to 3.7 times more D than 2–4 µm, but no clear dependence of the depth profile on irradiation conditions is visible. Consequently the NRA analysis catches most of the D retained in the W samples. Steels in contrast show mostly flat retention profiles, indicating a faster diffusion of D beyond the analysis depth. With a constant depth profile, the evolution of retention with DPA measured in D/m^2 becomes identical with the evolution of physical retention (measured in atom%, retention per m^3, or D/W) and is thus representative for the defect density. This study aims at determining physical retention in a region of interest for bulk material extrapolations, rather than plasma flux normalised values. Consequently, deuterium deeper than the region of interest, the NRA range of about 4 µm, will be neglected here and the given retention is not the total retention.

The surface near retention (in NRA range) increases strictly with damage up to 0.2 DPA in both W and steels. At this point the retention starts saturating. The lines drawn in Fig. 5 represent this with a good agreement to an exponential function with offset. This saturation retention level lies in W a factor 13–20 above the un-irradiated spots. In HiperFer steel, the increase lies between a factor 116–184. For Eu97 the data scatter significantly, probably due to a generally worse alignment of irradiation and analysis, since this was the first sample analysed and should therefore be neglected. Since the un-irradiated retention in

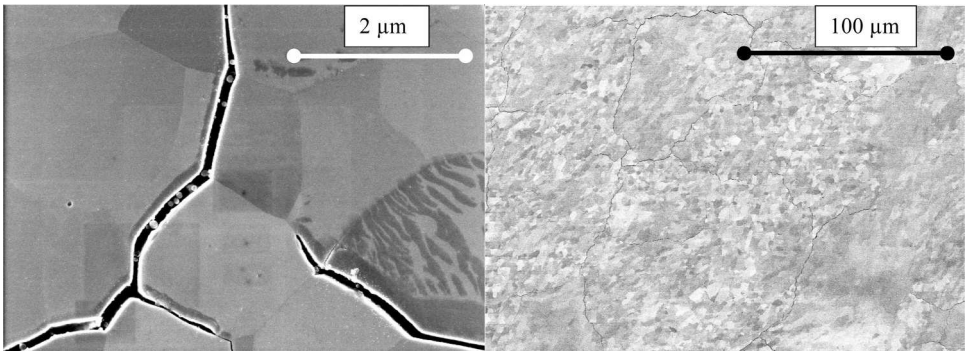

Fig. 4. Representative 5 kV SEM images of the same W sample spot irradiated to 0.02 DPA. Already at the lowest DPA levels crack networks appear, but remain unchanged with increasing DPA level. Possibly pre-existing stress lead to the cracking.

statement for steels and W. With increasing DPA, the damage progresses by increasing interaction strength between defects from the atomic scale (< 0.1 DPA) over the nano-scale up to macroscopic size (voids/bubbles) in the limit of very high DPA.

The measured hydrogen isotope retention allows for a rough extrapolation of the tritium retention in ITER and future devices. The data suggest a saturation of retention already at 0.2 DPA, therefore similar retention can be expected in a low DPA reactor as ITER (in D-T phase) and a high DPA future power reactor. In a power reactor, higher wall temperatures together with defect saturation potentially even reduce the retention compared to ITER with its coolant temperatures close to the temperatures of this study. For an extrapolation we assume a complete permeation of D/T through the plasma-facing components together with a flat depth profile using the above observed maximum retention of 3.2 (W) and 0.08 (HiperFer)% D, respectively. This assumption intends to approximate a case of high fluence long-time exposure with complete saturation of retention throughout the material. A plasma-facing component armour of 5 mm thickness and 800 m^2 (4 m^3 material) would exhibit a saturation retention limit of $4.05 \times 10^{27} T$ = 20.1 kg for a pure W armour and $1.36 \times 10^{26} T$ = 0.68 kg for a pure HiperFer armour, assuming 50% D and 50% T retention and displacement damage ≥ 0.2 DPA. These numbers neglect implantation, outgassing, and effects of transmutation damage, therefore representing mostly an upper limit of long-term operation. These numbers lie a factor 3 above the extrapolations at a factor 3 lower DPA values as stated for the ITER W-divertor with radiation damage in [1] (calculations in [1] were based on Mo values).

4. Conclusions

Focussed proton beam irradiation at about 3 MeV successfully produced relevant displacement damage in W and steels. We demonstrated a release of these samples to regular, non-active analysis and exposure facilities at least up to the order of 1 DPA (at the surface). Here the beam spot size and the production of Mn-54 (from the Cr content) and Co-57 (from the Fe content) represent the limiting factors with their long half-life and low release limits. As such focussed 3 MeV proton beams provide a valuable compromise between damage rate, handling, and similarity to neutron damage. Along with this, advantages in comparability and compatibility to non-irradiated studies are realized. On the downside, the range of damage stays ≤ 35 μm. This extends the range of applications beyond what is possible with heavy ions (typical range < 3 μm), enabling for example retention, indentation, or transient heat load tests of damaged samples with good damage homogeneity throughout the first grain scale. Consequently, macroscopic tests (~1 mm samples) of accelerator irradiated samples unavoidably require higher energies [8] and radiation protected environments, quickly reaching a complexity of analysis similar to neutron irradiation studies.

From the technical side, the beam heat limited the damage rates to a few DPA/day (~10^{-4} DPA/s) in the given setup due to temperature

[redacted]

ed out to be
udies due to
be either due
s or indicate
dicated by lit-
re required for

further insight into the nature of damage progression in particular when going to higher DPA.

The proton irradiation led to large increases in D retention even at low DPA. The results are compatible with a saturating (exponential) increase of the retention with DPA even at the investigated ~300 K. The saturating relation corresponds to an interacting population in which for example annihilation and clustering limit the defect concentration. Interestingly, the saturation onset at about 0.2 DPA and saturation retention quantity in the order of a few atom% D are consistent within errors to several heavy ion based irradiation studies, in spite of the presumed different damage evolution due to about 5 orders of magnitude higher cascade densities of heavy ions, according to SRIM. Only the heavy ion study [16] significantly differs with significantly lower retention in W, in spite of similar fluence and sample conditions. The low scaling with DPA in [16] indicates a retention dominated by surface near blisters (which are unaffected by DPA), while here and in the other considered studies relatively flat depth profiles within the damaged zone and strong DPA scalings indicate a retention in defects. Our irradiation produced surface cracks instead of blisters. The 10 times higher range of 3 MeV protons and the absence of implantation into the blister depth range allows excluding explanations based on implantation and damage cascade density due to the good correlation of our data with several heavy ion studies, e.g. [4,5]. In fusion devices we would expect a defect dominated retention due to the long plasma exposure times and high temperatures, supporting use of the higher D/W retention results for extrapolations. Lastly, since the exposures in this study were made slightly above room temperature, the results represent a limiting case of lowest defect mobility and highest long-term retention for fusion devices.

It remains an open question in how far ion irradiations induce damage comparable to D-T neutron irradiation, but the results of this study in conjunction with literature data boosts the confidence in intercomparability at least of different ion projectiles. Furthermore, the apparent independence of retention increase on cascade density indicates comparability of ion with neutron irradiations. In this way ion irradiation provides a prospect for providing solid extrapolations of hydrogen isotope retention in future fusion reactor materials. Consequently, this study demonstrated the value of focussed 3 MeV proton irradiation, opening up new fields for studying irradiated materials with optimal access to temperature, DPA, material types, and most importantly post-analysis. The main problem of non-existing D-T fusion representative irradiation experiments and the corresponding uncertainty of extrapolations of existing results towards fusion power reactor remains, but adding protons as a third method besides heavy ion and fission neutron studies gives a prospect for improving the physical understanding of radiation damage required for solid extrapolations. Extrapolating the presented results, which are consistent to literature, to future fusion reactors leads to T retention values exceeding the envisaged T limits at least for W in ITER D-T conditions in a worst case scenario. This result highlights the importance of further irradiation-retention studies to which 3 MeV proton studies could

interests or personal relationships that could have appeared to influence the work reported in this paper.

Acknowledgments

The authors thank the PSI-2 Team, especially Michael Vogel and Sebastian Kraus for the reliable device operation.

This work has been carried out within the framework of the EURO fusion Consortium and has received funding from the Euratom research and training programme 2014-2018 and 2019-2020 under grant agreement No 633053. The views and opinions expressed herein do not necessarily reflect those of the European Commission.

Supplementary materials

Supplementary material associated with this article can be found, in the online version, at doi:10.1016/j.nme.2020.100742.

References

[1] J. Roth, et al., Tritium inventory in ITER plasma-facing materials and tritium removal procedures, Plasma Phys. Control. Fusion 50 (10) (2008) 103001, , https://doi.org/10.1088/0741-3335/50/10/103001.

[2] M. Poon, A.A. Haasz, J.W. Davis, Modelling deuterium release during thermal

[9] ASTM Standard E521-96, Standard Practice For Neutron Radiation Damage Simulation By Charged-Particle Irradiation, (2009).

[10] R.E. Stoller, M.B. Toloczko, G.S. Was, A.G. Certain, S. Dwaraknath, F.A. Garner, On the use of SRIM for computing radiation damage exposure, Nucl. Instrum. Methods Phys. Res. Section B Beam Interact. Mater. Atoms 310 (2013) 75–80, https://doi.org/10.1016/j.nimb.2013.05.008.

[11] C. Björkas, K. Nordlund, S. Dudarev, Modelling radiation effects using the ab-initio based tungsten and vanadium potentials, Nucl. Instrum. Methods Phys. Res. Section B Beam Interact. Mater. Atoms 267 (18) (Sep. 2009) 3204–3208, https://doi.org/10.1016/j.nimb.2009.06.123.

[12] A. Kreter, et al., Linear plasma device PSI-2 for plasma-material interaction studies, Fusion Sci. Technol. 68 (1) (2015) 8–14, https://doi.org/10.13182/FST14-906.

[13] S. Möller, O. Kachko, M. Rasinski, A. Kreter, C. Linsmeier, In situ investigation of helium fuzz growth on tungsten in relation to ion flux, fluence, surface temperature and ion energy using infrared imaging in PSI-2, Phys. Scr. T170 (2017) 014017, , https://doi.org/10.1088/1402-4896/aa8a0a.

[14] V. Kh. Alimov, M. Mayer, J. Roth, Differential cross-section of the D(3He,p)4He nuclear reaction and depth profiling of deuterium up to large depths, Nucl. Instrum. Methods Phys. Res. Section B Beam Interact. Mater. Atoms 234 (3) (Jun. 2005) 169–175, https://doi.org/10.1016/j.nimb.2005.01.009.

[15] I. Gavish Segev, E. Yahel, I. Silverman, G. Makov, Blister formation at subcritical doses in tungsten irradiated by MeV protons, J. Nucl. Mater. 496 (Dec. 2017) 77–84, https://doi.org/10.1016/j.jnucmat.2017.09.024.

[16] W.R. Wampler, R.P. Doerner, The influence of displacement damage on deuterium retention in tungsten exposed to plasma, Nucl. Fusion 49 (11) (2009) 115023, , https://doi.org/10.1088/0029-5515/49/11/115023.

[17] Gary Was S., Fundamentals of Radiation Materials Science, Springer (2007).